# Aeroelastic Flutter and Divergence of Stiffness Coupled, Graphite/Epoxy Cantilevered Plates

Steven J. Hollowell*
*Flight Dynamics Laboratory, Wright-Patterson Air Force Base, Ohio*
and
John Dugundji†
*Massachusetts Institute of Technology, Cambridge, Massachusetts*

**An analytical and experimental investigation was conducted to determine the aeroelastic flutter and divergence behavior of unswept, rectangular wings simulated by graphite/epoxy, cantilevered plates with various amounts of bending-torsion stiffness coupling. The analytical approach incorporated a Rayleigh-Ritz energy formulation and unsteady, incompressible two-dimensional aerodynamic theory. Flutter and divergence velocities were obtained using the *V-g* method and compared to results of low-speed wind tunnel tests. Stall flutter behavior was also examined experimentally. There was good agreement between analytical and experimental results. Wings with negative stiffness coupling exhibited divergence, while positive coupling delayed the onset of stall flutter.**

## Introduction

AEROELASTIC tailoring is defined broadly as the technology to design a lifting surface which exhibits a desired aeroelastic response. Desired aeroelastic responses considered most often are maximization of flutter and divergence speeds, although other aeroelastic responses can be important depending on the application, such as control reversal speed, camber changes as a function of load and speed, and angle of attack changes as a function of load.

Aeroelastic tailoring, which exploits the anisotropic character of advanced composites, has received considerable attention in recent literature. Krone Jr.[1] concluded that forward-swept wings without divergence or weight penalties may be possible through the use of selectively laminated advanced composites. Weisshaar[2,3] analytically extended Krone's conclusion to potentially practical wing designs. Weisshaar concluded that the bending-torsion stiffness coupling of anisotropic advanced composite materials could be used to alleviate divergence in forward-swept wings. Sherrer et al.[4] conducted a series of wind tunnel tests using simple plate-like models of a forward-swept wing. These tests essentially verified Weisshaar's conclusion and also showed that existing analytical techniques (computer program) would adequately predict the divergence dynamic pressures for most test conditions.

Additional aeroelastic wind tunnel tests on specific forward-swept wing model designs were conducted by Wilkinson and Rauch[5] of Grumman Aircraft and Ellis et al.[6] of Rockwell North American Aircraft. A good general discussion of these efforts on forward-swept wings can be found in Ref. 7. More recently, effects of rigid body pitch modes on these wings have been explored by Weisshaar et al.[8] Still, there is only a limited amount of wind tunnel data available which examines the effect of structural bending-torsion coupling on flutter speed or that verifies the accuracy of analytical predictions. Additionally, the phenomenon of stall flutter has received only limited attention as it relates to metal lifting surfaces,[9,10] and virtually none as related to advanced composite lifting surfaces.

To add to the limited experimental data on aeroelastic tailoring with graphite/epoxy, an investigation was conducted to determine the effect of bending-torsion stiffness coupling

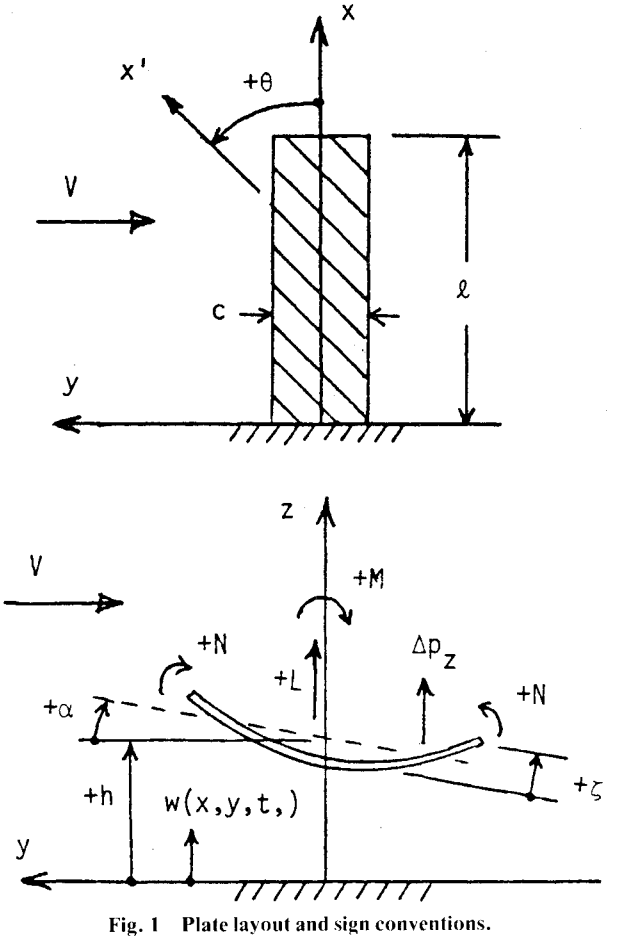


**Fig. 1 Plate layout and sign conventions.**

Presented as Paper 82-0722 at the 23rd Structures, Structural Dynamics, and Materials Conference, New Orleans, La., May 10-12, 1982; submitted May 28, 1982; revision received July 20, 1983. This paper is declared a work of the U.S. Government and therefore is in the public domain.

*Captain, USAF, Aeronautical Engineer. Member AIAA.
†Professor, Department of Aeronautics and Astronautics. Member AIAA.

on both the divergence and flutter velocities of unswept lifting surfaces in incompressible flow. Types of flutter examined included both potential flow (low angle of attack) and stall flutter. This paper summarizes the analysis design, and testing of six wind tunnel models with widely varying amounts of bending-torsion coupling. The models were of aircraft wings approximated by cantilevered, rectangular, flat plates constructed of graphite/epoxy with half-span aspect ratios of 4 (8, by standard aerodynamic convention). The present paper is based on an M.S. thesis by the first author.[11]

## Theory

### Anisotropic Plate Flexural Stiffness

The flexural modulus components $D_{ij}$ of a laminated advanced composite plate depend on both the fiber orientation and stacking sequence of the individual laminas. This development will consider only laminated plates with a midplane symmetric stacking sequence, due to the difficulties in fabricating flat unsymmetric laminated plates. The ply angles follow the sign convention in Fig. 1.

The in-plane, on-axis lamina modulus components $Q_{ij}$ were obtained from the orthotropic engineering constants for Hercules AS1/3501-6 unidirectional graphite/epoxy tape, from which the wind tunnel models were fabricated. These engineering constants take on different values depending on whether they are obtained from in-plane static tensile or out-of-plane flexural tests. Turner[12] explored this subject in detail and the engineering constants which he derived from out-of-plane, flexural loads were used for the analysis results presented in this paper. For comparison purposes, Table 1 presents the orthotropic engineering constants derived by Turner, along with standard values used by M.I.T. which were obtained from in-plane tests.

The flexural modulus $D_{ij}$ for an $n$-ply laminate with arbitrary ply angle orientation was obtained from the expression,[13]

$$D_{ij} = \sum_{k=1}^{n} Q_{ij}^{(\theta_k)} [z_k^3 - z_{k-1}^3]/3 \qquad i,j = 1,2,6 \tag{1}$$

where $Q_{ij}^{(\theta_k)}$ is the off-axis lamina modulus of the $k$th ply, $\theta_k$ the ply angle of the $k$th ply, and $z_k$ the distance up from the midplane to the upper surface of the $k$th ply.

Table 2 presents the flexural moduli $D_{ij}$ as computed for the six laminates used in the present investigation.

**Table 1 Orthotropic engineering constants**

| Property: (Hercules AS1/3501-6 graphite/epoxy) | In-plane loading | Out-of-plane loading |
|---|---|---|
| $E_L$, N/m$^2$ | $130\times10^9$ | $98\times10^9$ |
| $E_T$, N/m$^2$ | $10.5\times10^9$ | $7.9\times10^9$ |
| $\nu_{LT}$ | 0.28 | 0.28 |
| $G_{LT}$, N/m$^2$ | $6.0\times10^9$ | $5.6\times10^9$ |
| Ply thickness, $t_p$, m | $0.134\times10^{-3}$ | |
| Density, $\rho_G$, kg/m$^3$ | 1520 | |

### Rayleigh-Ritz Formulation

The direct Rayleigh-Ritz energy method is a relatively simple, straightforward approximation for plate deflections, as required for the free vibration, flutter, and divergence analyses in this paper. The "wing" was idealized by a rectangular cantilevered flat plate with uniform thickness.

The Rayleigh-Ritz analysis assumes a deflection shape for the structure. Since the first three vibration modes would probably be of most interest for flutter analysis, a five-term deflection equation was chosen. These five terms approximated the plate deflection for the first bending (1B), second bending (2B), first torsion (1T), second torsion (2T), and first chordwise (1C) vibration modes. Originally only the first three terms were taken, but later it was shown by Jensen et al.[14,15] that the last two terms were necessary to improve the accuracy of the approximations for the first three vibration modes. The deflection equation, written in generalized coordinates, is

$$w = \sum_{i=1}^{5} \gamma_i(x,y)\, q_i(t) \tag{2}$$

where $w$ is the lateral deflection, $\gamma\epsilon_i(x,y)$ the nondimensional deflection or mode shape of the $i$th mode, and $q_i(t)$ the generalized displacement of the $i$th mode. All of the mode shapes satisfy the geometric boundary conditions for a cantilevered plate, and the generalized displacement has units of length and is a function only of time. For convenience and consistency, the sign conventions in Fig. 1 were used for development of all analysis methods.

The mode shape can be written as

$$\gamma\epsilon_i(x,y) = \phi_i(x)\psi_i(y) \qquad i = 1,\ldots,5 \tag{3}$$

where $\phi$ and $\psi$ are single-dimension mode shapes in the $x$ and $y$ directions, respectively. The mode shapes used in this paper are shown below.

$$\begin{aligned}
&\phi_1(x) = \text{first cantilever beam mode}\\
&\phi_2(x) = \text{second cantilever beam mode}\\
&\phi_3(x) = \sin(\pi x/2l)\\
&\phi_4(x) = \sin(3\pi x/2l)\\
&\phi_5(x) = x/l(1-x/l)\\
&\psi_1(y) = 1\\
&\psi_2(y) = 1\\
&\psi_3(y) = y/c\\
&\psi_4(y) = y/c\\
&\psi_5(y) = [4(y/c)^2 - 1/3]
\end{aligned} \tag{4}$$

The strain energy $U$ for a symmetric anisotropic laminate is[16]

$$\begin{aligned}
U = \tfrac{1}{2}\int_0^l \int_{-c/2}^{c/2} [&D_{11}(w_{,xx})^2 + 2D_{12} w_{,xx} w_{,yy}\\
&+ D_{22}(w_{,yy})^2 + 4D_{16} w_{,xx} w_{,xy} + 4D_{26} w_{,yy} w_{,xy}\\
&+ 4D_{66}(w_{,xy})^2]\,dy\,dx
\end{aligned} \tag{5}$$

**Table 2 Flexural moduli for laminates[a]**

| Laminate | $D_{11}$ | $D_{12}$ | $D_{16}$ | $D_{22}$ | $D_{26}$ | $D_{66}$ |
|---|---|---|---|---|---|---|
| $[0_2/90]_s$ | 4.125 | 0.096 | 0 | 0.490 | 0 | 0.243 |
| $[\pm45/0]_s$ | 1.550 | 0.928 | 0.437 | 1.404 | 0.437 | 1.075 |
| $[+45_2/0]_s$ | 1.550 | 0.928 | 0.946 | 1.404 | 0.946 | 1.075 |
| $[-45_2/0]_s$ | 1.550 | 0.928 | −0.946 | 1.404 | −0.946 | 1.075 |
| $[+30_2/0]_s$ | 2.704 | 0.720 | 1.180 | 0.666 | 0.459 | 0.866 |
| $[-30_2/0]_s$ | 2.704 | 0.720 | −1.180 | 0.666 | −0.459 | 0.866 |

[a] All values in N-m.

where a comma denotes partial differentiation. The kinetic energy $T$ for the plate is

$$T = \tfrac{1}{2}\int_0^l \int_{-c/2}^{c/2} m\dot{w}^2 \,dy\,dx \tag{6}$$

where $(\dot{}) = d/dt, m = \rho_G t_G$ is the mass/area, $\rho_G$ the density of graphite/epoxy, and $t_G$ the total plate thickness. The change in external work $\delta W_e$ can be expressed as

$$\delta W_e = \int_0^l \int_{-c/2}^{c/2} \Delta p_z \delta w \,dy\,dx \tag{7}$$

where $\Delta p_z$ is a distributed lateral load per unit area.

Placing the previous expressions into Lagrange's equations results in the five equations of motion,

$$[M]\ddot{q} + [K]q = Q = \pi\rho\omega^2 b^3 [A]q \tag{8}$$

where $[K]$ and $[M]$ are the appropriate stiffness and mass matrices resulting from the strain and kinetic energies, and $Q$ represents the harmonic sinusoidal aerodynamic forces resulting from the pressure distribution $\Delta p_z$ in the external work term. Specific values for the $K$, $M$, and $A$ elements can be found in an earlier version of this paper.[17] Two points should be mentioned in the analysis: 1) the stiffness elements $K_{ij}$ of the two uncoupled torsional modes were corrected for root warping restraints by using the structural aspect ratio correction factors $k_{1T}$ and $k_{2T}$ of Crawley and Dugundji[18] given in Table 3, and 2) the analysis used two-dimensional, incompressible, unsteady aerodynamic strip theory,[19] and included camber change effects as adapted from Spielberg.[20]

#### Free Vibration Analysis

The free vibration problem was formulated by setting the generalized forces $Q_i$ equal to zero in Eq. (8). Assuming harmonic (sinusoidal) motion, the generalized displacements can be expressed as

$$q = qe^{i\omega t} \qquad \ddot{q} = -\omega^2 qe^{i\omega t} \tag{9}$$

where $\omega$ is the frequency. These expressions, when substituted into the differential equations of motion, Eq. (8), result in the real eigenvalue problem,

$$\{[K] - \omega^2 [M]\}q = 0 \tag{10}$$

Equation (10) is solved for the eigenvalues $\omega_i^2$ and associated eigenvectors $q_i$. Then the natural vibration frequencies $\omega_i$ are found from $\omega_i = \sqrt{\omega_i^2}$, while the associated vibration mode shapes are found by substituting $q_i$ back into Eq. (2).

#### Aeroelastic Flutter Analysis

The flutter analysis was done using the familiar $V$-$g$ method.[19] The structural damping coefficient $g$, introduced into the equations of motion, represents the amount of damping that must be added to the structure to attain neutral stability (flutter) at the given velocity. Negative values of structural damping indicate the structure is stable, while positive values indicate instability. Flutter occurs when the structural damping coefficient $g$ equals the actual damping of the structure.

Assuming harmonic motion $q = qe^{i\omega t}$, the equations of motion [Eq. (8)] are rearranged into the form,

$$\{[B] - Z[K]\}q = 0 \tag{11}$$

where

$$[B] = [M] + \pi\rho b^3 [A] \qquad Z = (1 + ig)/\omega^2 \tag{12}$$

For given values of reduced frequency, $k = \omega b/V$, the complex coefficients $A$ are evaluated, and together with $M$ and $K$ are placed into Eq. (11) which is solved for the five complex eigenvalues $Z$. From these eigenvalues and from $k$, the $\omega$, $g$, and $V$ are determined. Plots of $g$ and $\omega$ vs $V$ then characterize the flutter stability and frequencies of the wing. The $\omega$ values at $V \sim 0$ represent the natural frequencies with air mass effects present. The natural frequencies in a vacuum were also obtained from Eq. (12) by using a small value of air density and a large value of $k$.

#### Divergence

Divergence, a static deflection phenomenon in which the aerodynamic forces on the wing exceed the elastic restoring forces of the wing, can also be obtained from the $V$-$g$ diagram. It is characterized there by the structural damping of a deflection branch going abruptly from a negative value to zero (but not crossing the $V$ axis) at the same time the frequency goes to zero.

For the divergence analysis, the lift curve slope $\partial C_l/\partial\alpha = 2\pi$ was empirically reduced by the factor $\mathcal{R}/(\mathcal{R}+2)$ to account for the effects of finite span, as suggested in Ref. 19. Here $\mathcal{R}$ is the aspect ratio $2l/c$ of the wing. This is equivalent to modifying the divergence velocity $V_D$ found from the $2\pi$ lift curve slope as shown below.

$$(V_D)_{\mathcal{R}} = \sqrt{(\mathcal{R}+2)/\mathcal{R}}\,(V_D)_{2\pi} \tag{13}$$

The above aspect ratio correction was not used for the flutter speed calculations.

Alternatively, for the divergence calculations, the divergence speed was also calculated directly by neglecting the mass term $[M]$ in Eq. (8) and rearranging the equations into the form

$$\{[A^{\text{stat}}] - \lambda[k]\}q = 0 \tag{14}$$

where

$$[A^{\text{stat}}] = \lim_{k\to 0} \{k^2 [A]\} \qquad \lambda = 1/\pi\rho V^2 b \tag{15}$$

In the above, $[A^{\text{stat}}]$ are now all real coefficients. The largest positive eigenvalue $\lambda$ gives the lowest divergence speed $V_D$. Again, $V_D$ was corrected for finite aspect ratio by applying Eq. (13).

**Table 3 Structural aspect ratio corrections**

| Laminate | $\beta$[a] | $k_{1T}$ | $k_{2T}$ |
|---|---|---|---|
| $[\pm 0_2/90]_s$ | 0.0221 | 1.87 | 6.30 |
| $[\pm 45/0]_s$ | 0.0019 | 1.63 | 5.00 |
| $[+45_2/0]_s$ | 0.0019 | 1.63 | 5.00 |
| $[-45_2/0]_s$ | | | |
| $[+30_2/0]_s$ | 0.0041 | 1.68 | 5.20 |
| $[-30_2/0]_s$ | | | |

[a] $\beta = D_{11}/48D_{66}(l/c)^2$.

## Experiment

#### Model Design and Fabrication

The wind tunnel model was conceived as a half-span representation of an aircraft wing using a plate cantilevered at the base. Model design was driven by several constraints imposed by the study objectives and available facilities. The models had to

1) demonstrate a wide range of bending-torsion coupling;

2) be rectangular shaped, constant thickness flat plates with zero sweep;

3) exhibit flutter within the 32 m/s velocity limitation of the wind tunnel;

4) be small enough to be constructed with the available equipment for cutting and curing graphite/epoxy at M.I.T.; and

5) be tough enough to withstand repeated large static and oscillatory loads.

Constraints 3 and 4 directly opposed one another and drove the design to a very thin laminate, which increased the possibility of warping during curing. Constraint 1 seemed to indicate that an unbalanced but midplane symmetric lamination was desirable. This also increased the possibility of warping during curing.

The total thickness finally chosen was six plies. Five different laminates were selected as representative of a wide range of bending-torsion coupling stiffnesses, both positive and negative. The first two laminates, $[+30_2/0]_s$ and $[-30_2/0]_s$, were chosen because they exhibited the highest theoretical bending-torsion stiffness $D_{16}$, but still had a large $D_{66}$. The final laminate, $[0_2/90]_s$, was chosen because it exhibited the highest bending stiffness $D_{11}$ and zero $D_{16}$. During the test program another laminate, $[\pm 45/0]_s$, was added because it had the same theoretical $D_{11}$ and $D_{66}$ as $[+45/_20]_2$ with less $D_{16}$. To minimize the number of test specimens which had to be constructed, the $[+\theta_2/0]_s$ and $[-\theta_2/0]_s$ test specimens were actually the same laminate simply rotated 180 deg about the $x$ axis (see Fig. 1).

Each model had an overall length of 330 mm (13 in.) and a chord of 76 mm (3 in.). The overall length included a 25 mm (1 in.) loading tab, making the effective cantilever plate length 305 mm (12 in.). This gave the plate an aspect ratio ($l/c$) of 4. Finally, in an effort to minimize plate stiffness, an airfoil shaped fairing was not used for these wind tunnel tests.

Individual plies were manually cut from Hercules ASI/3501-6 graphite/epoxy prepreg tape and layed up into $305 \times 356$ mm laminates, which were cured in an autoclave. Models were cut from the laminates using a diamond cutting wheel mounted on an automatic feed milling machine. Loading tabs were machined from a 2.4 mm aluminum plate and epoxied to the base of each model. Bending and torsion strain gages were attached to the base of both sides of each model at the midchord. The gages were wired to compensate for temperature changes during tests. Prior to attaching the strain gages and loading tabs each model was measured (thickness, width, and length), weighed, and checked for warping. These figures were recorded and compared to nominal (theoretical) values.

#### Vibration Test Apparatus

A vise machined from a $25.4 \times 152 \times 29$ mm aluminum block was suspended by four spring steel strips, allowing it to translate in the z direction (Fig. 1), but restricting motion in all other directions. This vise was attached to an electromagnetic shaker driven by an audio amplifier. A frequency generator with a digital readout provided the input signal. The shaker had a rated frequency range of 5-3000 Hz.

#### Wind Tunnel Test Apparatus

All wind tunnel tests were performed in the M.I.T. Department of Aeronautics and Astronautics acoustic wind tunnel. The acoustic wind tunnel is a continuous-flow tunnel with a $1.5 \times 2.3$ m ($5 \times 7.5$ ft) free jet test section 2.3 m (7.5 ft) long, located inside a large anechoic chamber. The tunnel has a velocity range of 0-32 m/s (0-105 ft/s), which is read from an alcohol manometer.

The test apparatus (see Fig. 2) consisted of a turntable machined from aluminum and mounted on a 635-mm tall pedestal made of 152-mm-diam steel pipe. The pedestal was mounted directly to a rigid platform in the floor of the test section. The vise from the free vibration test apparatus was fastened to the turntable and was covered by a wooden disk to provide smooth airflow past the model. Angle of attack graduation (2-deg increments) were marked on the disk and the turntable was rotated during the tests by an aluminum push rod extending outside the test section. The model was mounted in a vertical position to eliminate any gravity effects. The instrumentation system was a Gould 2400 series four-channel stripchart recorder which had an internal time base generator and recorded the bending and torsion strains of the model.

#### Test Procedures

The first three vibration modes were obtained by slowly increasing the frequency and visually identifying when the amplitude of each mode peaked. The frequency at this condition was then read from the counter. The free vibration tests were repeated several times to ensure consistent results.

The wind tunnel tests began by exciting the first bending and torsion modes of the model under zero velocity conditions. The resulting damped oscillations were recorded on the stripchart. The model was set at zero angle of attack and the wind tunnel run up and stabilized at the first velocity. The angle of attack was then varied from +18 to −18 deg, with a stripchart record being made at 2-deg increments. The model was reset to zero angle of attack, the velocity increased, and after it stabilized, the angle of attack sweep was repeated. This procedure was repeated until the mode either fluttered or diverged at zero angle of attack or the maximum speed of the wind tunnel was reached. Divergence was noted when the angle of attack could not be set small enough to keep the wing from flipping over to either one side or the other.

Divergence testing often results in the destruction of a model. To avoid this, wind tunnel speeds were increased in very small increments as the divergence velocity was approached. The model deflections were monitored closely, and when it would no longer return to a zero deflection state, the tunnel velocity was not increased further. Because the models were rather flexible, they proved very robust and after many tests, not a single one was lost.

All data reduction was done manually (with the aid of a programmable calculator). Flutter frequencies were annotated on the stripchart along with the velocity. On selected stripchart records, peak-to-peak amplitudes of both bending and torsion strain gages were annotated. Finally, the flutter boundary velocities were plotted vs angle of attack for each model.

## Discussion of Results

#### Free Vibration Tests

Table 4 gives the experimental and calculated natural frequencies of the six laminates tested. Comparing the experimental frequencies of the balanced laminate $[\pm 45/0]_s$ and the unbalanced laminate $[+45_2/0]_s$, one observes that

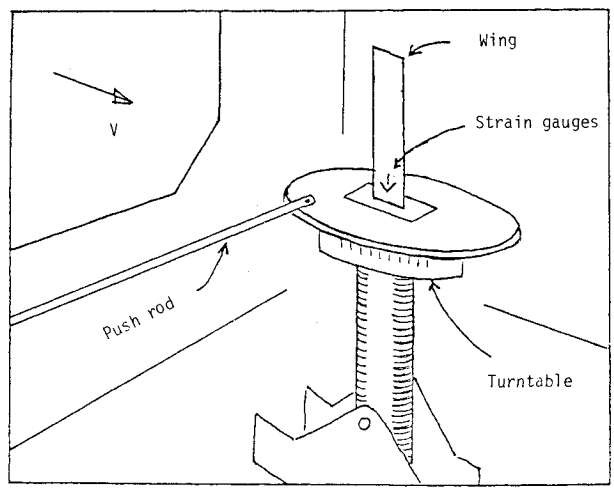


Fig. 2 Test setup in wind tunnel.

**Table 4 Natural frequencies of models**

| Model | Vibration mode | Experimental frequency, Hz | Calculated Frequency, Hz 5 modes | Calculated Frequency, Hz 3 modes |
|---|---|---|---|---|
| $[0_2/90]_s$ | 1B | 11.1 | 10.7 | 11.1 |
| | 1T | 42 | 39 | 33 |
| | 2B | 69 | 67 | 69 |
| | 2T | | 132 | |
| | 1C | | 430 | |
| $[\pm 45/0]_s$ | 1B | 6.1 | 5.7 | 6.4 |
| | 2B | 38 | 37 | 42 |
| | 1T | 77 | 69 | 70 |
| | 2T | | 216 | |
| | 1C | | 746 | |
| $[\pm 45_2/0]_s$ | 1B | 4.8 | 4.6 | 4.7 |
| $[-45_2/0]_s$ | 2B | 30 | 32 | 41 |
| | 1T | 51 | 55 | 71 |
| | 2T | | 205 | |
| | 1C | | 751 | |
| $[+30_2/0]_s$ | 1B | 6.0 | 6.0 | 5.8 |
| $[-30_2/0]_s$ | 2B | 36 | 41 | 52 |
| | 1T | 58 | 60 | 66 |
| | 2T | | 196 | |
| | 1C | | 542 | |

**Table 5 Zero-angle-of-attack flutter velocities**

| Model | Flutter velocity, m/s Experimental | Flutter velocity, m/s Calculated | Flutter frequency, Hz Experimental | Flutter frequency, Hz Calculated |
|---|---|---|---|---|
| $[0_2/90]_s$ | 25 | 21.0 | ~29 | 25 |
| $[\pm 45/0]_s$ | >32 | 39.0 | not obtained | 39 |
| $[+45_2/0]_s$ | 28 | 27.8 | ~24 | 28 |
| $[-45_2/0]_s$ | divergence | 27.8 | divergence | 27 |
| $[+30_2/0]_s$ | 27 | 27.8 | ~28 | 31 |
| $[-30_2/0]_s$ | divergence | 30.0 | divergence | 29 |

**Table 6 Divergence velocities**

| Model | Divergence velocity, m/s Experimental | Calculated ($C_{l_\alpha} = 2\pi$) | Calculated ($C_{l_\alpha} = 2\pi R/R+2$) |
|---|---|---|---|
| $[0_2/90]_s$ | flutter | 22.3 | 25.0 |
| $[\pm 45/90]_s$ | >32.0 | infinite, | no divergence |
| $[+45_2/0]_s$ | flutter | infinite, | no divergence |
| $[-45_2/0]_s$ | 12.5 | 9.9 | 11.1 |
| $[+30_2/0]_s$ | flutter | infinite, | no divergence |
| $[-30_2/0]_s$ | 11.7 | 10.2 | 11.5 |

the frequencies of the first three vibration modes were lower for the unbalanced laminate. Since the theoretical bending stiffness $D_{11}$, torsion stiffness $D_{66}$, and chordwise stiffness $D_{22}$, were the same for both of these models (see Table 2), the differences in frequencies could be attributed entirely to the coupling stiffnesses $D_{16}$ and $D_{26}$. This stiffness coupling apparently reduces both the bending and torsion frequencies of the wing.

As shown in Table 4, the Rayleigh-Ritz analysis using the five modes given in Eqs. (2-4) gave generally good agreement with experiment. These frequencies were obtained using the $V$-$g$ method at large values of $k$, and, hence, had a small correction for virtual air mass present also. As mentioned earlier, a previous analysis which included only the first three modes 1B, 2B, and 1T, did not predict the coupled 2B and couled 1T modes adequately. These results are also shown in Table 4. This vibration problem was later resolved by Jensen et al.[14,15] and led to the present five-mode formulation. It should be noted also that the earlier three-mode analysis did not include the additional root warping correction $k_{1T}$, and, hence, the frequencies would have been somewhat higher had this $k_{1T}$ correction been used. (In fact, all of the three-mode frequencies then would have been higher than the corresponding five-mode frequencies.)

#### Wind Tunnel Tests

The primary objective of the wind tunnel tests was to obtain zero-angle-of-attack flutter and divergence velocities for each model, which could be compared to analytical results. The secondary objective was to examine the stall flutter behavior of each model. Since the test velocities were low and the models quite flexible, the onset of flutter at zero angle of attack tended to be gradual. For consistency, the flutter threshold was defined to be the velocity where the oscillation amplitude stabilized and the waveform became periodic. Determining the threshold for stall flutter was somewhat easier, because oscillation tended to begin abruptly when the stall angle of attack was reached.

The type of flutter (bending, torsion, or bending-torsion) could not be determined completely from the amplitude of the bending and torsion stripchart channels, since for a plate with bending-torsion coupling, the bending and torsion motions are mixed together. Accordingly, it was decided to define bending flutter as oscillation with a frequency very close to one of the bending natural frequencies, torsion flutter when the frequency was close to the torsion natural frequency, and bending-torsion flutter when the frequency was between the two.

The flutter threshold velocity is plotted vs root angle of attack in Fig. 3. The $[0_2/90]_s$ model, with no bending-torsion coupling, exhibited bending-torsion flutter at low angles of attack and torsion stall flutter at higher angles of attack. This behavior, showing a large drop in flutter speed with root angle of attack, is similar to that reported earlier by Rainey[9] for thin aluminum wings of 2 and 4% thickness ratios. The models with large positive bending-torsion coupling, $[+30_2/0]_s$ and $[+45_2/0]_s$, exhibited primarily bending-torsion flutter. The flutter velocity here did not drop significantly with increasing root angle of attack probably because the coupling caused a decrease in the top angle of attack, preventing it from stalling. However, at a root angle of attack of 18 deg, the flutter speed for the $[+30_2/0]_s$ model did drop significantly, and the flutter changed to torsion stall flutter. The $[\pm 45/0]_s$ model, which was stiff in torsion and had only a small amount of positive bending-torsion coupling, would not flutter at zero angle of attack within the 32 m/s maximum speed for the wind tunnel. However, at angles of attack above 8 deg it behaved similar to the $[0_2/90]_s$ model and exhibited torsion stall flutter. The models with large negative bending-torsion coupling, $[-30_2/0]_s$ and $[-45_2/0]_s$, exhibited divergence at zero angle of attack, and primarily bending stall flutter at root angles of attack greater than 1 deg. This flutter was due to bending motion causing the blade to stall due to the bending-torsion stiffness coupling.

To illustrate more clearly how the direction of the angle plies determines the behavior of the model, wind tunnel data for the three models with 45° plies are presented in Fig. 4. These three models have vastly different aeroelastic behavior. The $[\pm 45_2/0]_s$ indicated torsion stall flutter, the $[+45_2/0]_s$ indicated bending-torsion flutter and the $[-45_2/0]_s$ indicated divergence at zero angle of attack and bending stall flutter at higher angles of attack.

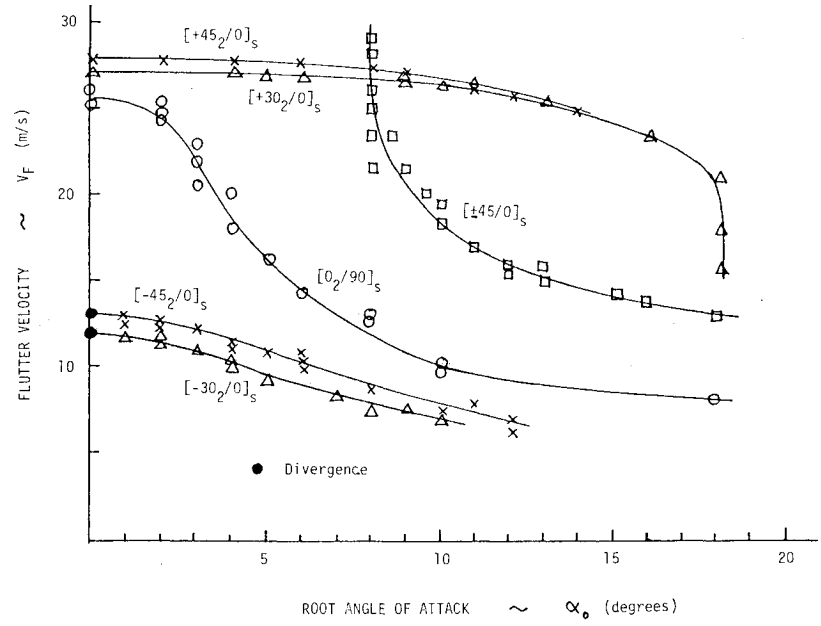


Fig. 3 Experimental flutter and divergence for all plates.

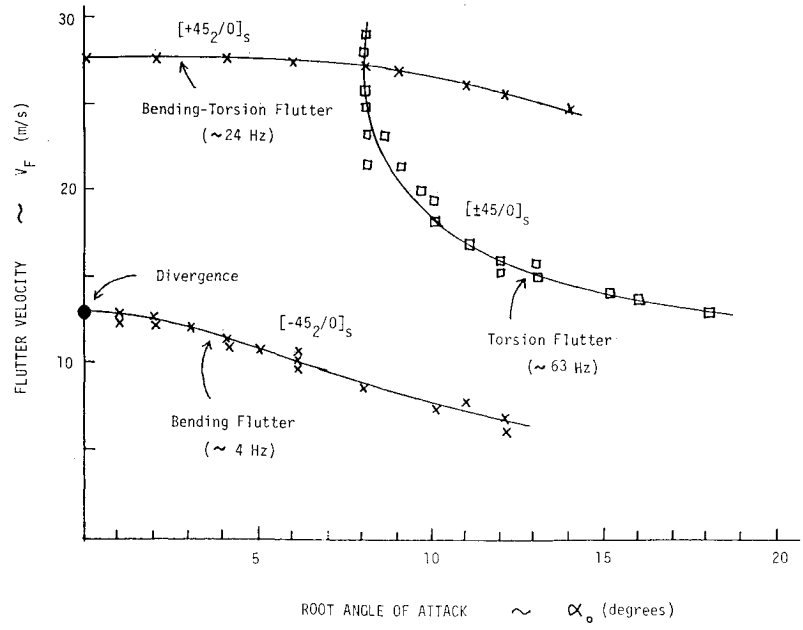


Fig. 4 Experimental flutter and divergence for 45 deg ply plates.

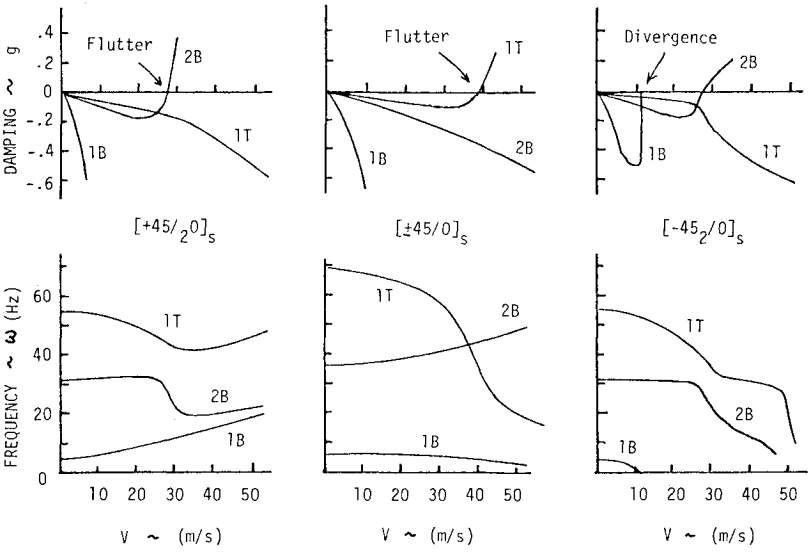


Fig. 5 Theoretical $V$-$g$ and $V$-$\omega$ diagrams for 45 deg ply plates.

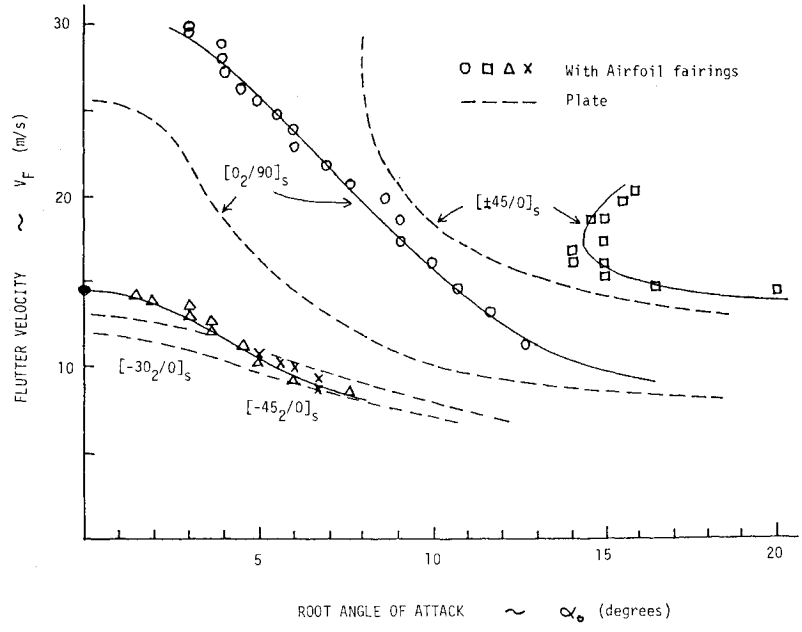


**Fig. 6 Effect of airfoil fairings on flutter and divergence.**

The vastly different low-angle-of-attack behavior observed in the wind tunnel data for these models was also evident in the theoretical analysis. The $V$-$g$ and $V$-$\omega$ diagrams are shown in Fig. 5 for the $[+45_2/0]_s$, $[\pm 45/0]_s$ and $[-45_2/0]_s$ models. The torsion branch became unstable on the $[0_2/90]_s$ model and apparently on the $[\pm 45/0]_s$ model, while the second bending branch became unstable on the $[+45_2/0]_s$ model. The $V$-$g$ and $V$-$\omega$ diagrams for the $[-45_2/0]_s$ model exhibited the classical first bending mode divergence. The remaining fourth and fifth mode branches are not shown in Fig. 5 since they always show a small stable negative $g$ over the velocity range indicated. One should note that the $V$-$g$ and $V$-$\omega$ diagrams are valid only for low-angle-of-attack flutter or divergence.

The calculated and experimental zero-angle-of-attack flutter velocities appear in Table 5. There was good agreement between analytical and experimental results for all cases in which a comparison could be made. The excellent agreement between analytical and experimental results for the $[+45_2/0]_s$ and $[+30_2/0]_s$ models is perhaps a bit fortuitous, but one may conclude that the analytical method appeared to provide a reasonable estimate for flutter velocities of the models in this paper. Both the experiments and the analyses showed the flutter velocities of the $[+45_2/0]_s$ and $[+30_2/0]_s$ models to be almost identical.

The calculated and experimental divergence velocities appear in Table 6. As with the flutter velocities, there was generally good agreement between experimental and analytical results (with finite span correction). Analysis results indicated that all models in this paper with positive stiffness coupling have an infinite divergence velocity. In examining the calculated $V$-$g$ diagram for the $[0_2/90]_s$ model, the authors observed that flutter occurred at a velocity of 21 m/s followed closely by divergence at 25 m/s. In the wind tunnel, the flutter occurring first probably obscured the divergence behavior. The $[-45_2/0]_s$ model had a slightly higher divergence velocity than the $[-30_2/0]_s$ model, while the analysis yielded a slightly opposite trend.

The stall flutter behavior of these flexible flat plate "airfoils" was checked at a later date by Selby.[21] He covered these same wings with smooth styrofoam airfoil fairings of 12% thickness ratio, and repeated these tests. The results are shown in Fig. 6. The airfoil fairings increased the stiffness slightly and moved the center of gravity forward, thereby increasing the flutter speed somewhat so that the $[+30_2/0]_s$ and $[+45_2/0]_s$ wings did not flutter in the range of the tunnel. However, the remaining results of these airfoil contoured wings are all qualitatively similar to those of the present investigation.

## Conclusions

Bending-torsion coupling can be beneficial in delaying or eliminating divergence. This stiffness coupling also can be employed to delay the onset of stall flutter by causing tip stall of a wing to occur at a higher root angle of attack. The approximate analysis methods adapted for use in this paper predicted natural vibration frequencies, flutter velocities, and divergence velocities with reasonable accuracy, except for some slight differences in divergence speed trends for small variations in bending-torsion coupling. The analytical $V$-$g$ diagrams for these models showed that the presence of positive bending-torsion coupling switched the unstable flutter branch from torsion to second bending mode, while negative bending-torsion coupling caused a divergence instability in the first bending mode.

Wind tunnel tests on a series of rectangular straight wings with varying bending-torsion coupling showed the widely varying aeroelastic behavior possible due to this stiffness coupling. Divergence instabilities and bending-torsion flutter occurred for low angles of attack while torsion stall flutter and bending stall flutter occurred at high angles of attack. There was reasonable agreement with theory at low angles of attack for the divergence and bending-torsion flutter. Torsion stall flutter occurred on wings with little or positive bending-torsion coupling, while bending stall flutter occurred on wings with negative coupling. The wind tunnel tests gave additional insights into the stall flutter behavior of flexible wings, which had been pointed out earlier by Rainey.[9]

Additional tests are in progress for wings with variable sweep to check the combined effects of bending-torsion coupling, stall behavior, and sweepback and sweepforward.

## Acknowledgments

The authors wish to acknowledge the support of the United States Air Force and the Materials Laboratory of Air Force Wright Aeronautical Laboratories for work conducted under Contract F33615-77-C-5155.

## References

[1]Krone, N.J. Jr., "Divergence Elimination with Advanced Composites," AIAA Paper 75-1009, 1975.

[2]Weisshaar, T.A., "The Influence of Aeroelasticity on Swept Composite Wings," AFWAL-TR-80-3137, Nov. 1980.

[3]Weisshaar, T.A., "Aeroelastic Tailoring of Forward Swept Composite Wings," *Journal of Aircraft*, Vol. 18, Aug. 1981, pp. 669-676.

[4]Sherrer, V.C., Hertz, T.J., and Shirk, M.H., "Wind Tunnel Demonstration of Aeroelastic Tailoring Applied to Forward Swept Wings," *Journal of Aircraft*, Vol. 18, Nov. 1981, pp. 976-983.

[5]Wilkinson, K. and Rauch, F., "Predicted and Measured Divergence Speeds of an Advanced Composite Forward Swept Wing Model," AFWAL TR-80-3059, July 1980.

[6]Ellis, J.W., Dobbs, S.K., and Miller, G.D., "Structural Design and Wind Tunnel Testing of a Forward Swept Fighter Wing," AFWAL TR-80-3073, July 1980.

[7]Hertz, T.J., Shirk, M.H., Ricketts, R.H., and Weisshaar, T.A., "On the Track of Practical Forward Swept Wings," *Astronautics & Aeronautics*, Vol. 20, Jan. 1982, pp. 40-53.

[8]Weisshaar, T.A., Zeiler, T.A., Hertz, T.J., and Shirk, M.H., "Flutter of Forward Swept Wings, Analyses and Tests," *Proceedings of the 23rd AIAA/ASME/ASCE/AHS Structures, Structural Dynamics, and Materials Conference*, New Orleans, La., May 1982, pp. 111-121.

[9]Rainey, G.A., "Preliminary Study of Some Factors which Effect the Stall-Flutter Characteristics of Thin Wings," NACA TN-3622, March 1956.

[10]Dugundji, J. and Aravamudan, K., "Stall Flutter and Nonlinear Divergence of a Two-Dimensional Flat Plate Wing," M.I.T. Aeroelastic and Structures Research Laboratory, Cambridge, Mass., ASRL-TR-159-6, July 1974.

[11]Hollowell, S.J., "Aeroelastic Flutter and Divergence of Graphite/Epoxy Cantilevered Plates with Bending-Torsion Stiffness Coupling," M.S. Thesis, M.I.T. Department of Aeronautics and Astronautics, Cambridge, Mass. Jan. 1981.

[12]Turner, M.D., "Comparison of Static and Dynamic Test Methods for Determining the Stiffness Properties of Graphite/Epoxy Laminates," M.S. Thesis, M.I.T. Department of Aeronautics and Astronautics, Cambridge, Mass., June 1979.

[13]Tsai, S.W. and Hahn, H.T., *Introduction to Composite Materials*, Technomic Publishing Co., Westport, Conn., 1980.

[14]Jensen, D.W., "Natural Vibration of Cantilever Graphite/Epoxy Plates with Bending-Torsion Coupling", M.S. Thesis, M.I.T. Department of Aeronautics and Astronautics, Cambridge, Mass., Aug. 1981.

[15]Jensen, D.W., Crawley, E.F., and Dugundji, J., "Vibration of Cantilevered Graphite/Epoxy Plates with Bending-Torsion Coupling," *Journal of Reinforced Plastics and Composites*, Vol. 1, July 1982, pp. 254-269.

[16]Ashton, J.E. and Whitney, J.M., *Theory of Laminated Plates*, Technomic Publishing Co., Stamford, Conn., 1970.

[17]Hollowell, S.J. and Dugundji, J., "Aeroelastic Flutter and Divergence of Stiffness Coupled, Graphite/Epoxy, Cantilevered Plates," *Proceedings of the 23rd AIAA/ASME/ASCE/AHS Structures, Structural Dynamics, and Materials Conference*, New Orleans, La., May 1982, pp. 416-426.

[18]Crawley, E.F. and Dugundji, J., "Frequency Determination and Non-Dimensionalization for Composite Cantilever Plates," *Journal of Sound and Vibration*, Vol. 72, No. 1, Sept. 1980, pp. 1-10.

[19]Bisplinghoff, R.L., Ashley, H., and Halfman, R.L., *Aeroelasticity*, Addison-Wesley Publishing Co., Reading, Mass., 1955.

[20]Spielberg, I.N., "The Two-Dimensional Incompressible Aerodynamic Coefficients for Oscillatory Changes in Airfoil Camber," *Journal of the Aeronautical Sciences*, Vol. 20, June 1953, pp. 432-434.

[21]Selby, H., "Aeroelastic Flutter and Divergence of Graphite/Epoxy Wings with Bending-Torsion Coupling," M.S. Thesis, M.I.T. Department of Aeronautics and Astronautics, Cambridge, Mass., Jan. 1982.